Catalysis Science & Technology

ROYAL SOCIETY OF CHEMISTRY

PAPER

View Article Online
View Journal

Published on 29 October 2020. Downloaded by University of New England on 11/9/2020 7:05:56 PM.

Check for updates

Cite this: DOI: 10.1039/d0cy01675f

# Galvanic synthesis of AgPd bimetallic catalysts from Ag clusters dispersed in a silica matrix†

V. Sudheeshkumar,[a] Maryam Alyari,[a] Mahesh Gangishetty[b] and Robert W. J. Scott *[a]

Received 25th August 2020,
Accepted 29th October 2020

DOI: 10.1039/d0cy01675f

rsc.li/catalysis

While bottom-up synthetic strategies for the formation of near-monodisperse clusters have attracted much attention, top-down synthetic strategies in which metals are dispersed into clusters can also be viable. In this study, we follow up previous work that showed the formation of Ag clusters dispersed in a silica matrix by breaking up larger triangular Ag nanoparticles upon calcination in air. AgPd bimetallic catalysts were synthesized *via* a galvanic replacement reaction of these thermally activated Ag clusters in a silica matrix. The galvanic reaction of the Ag clusters with Pd(II) salts was monitored by *in situ* XANES spectroscopy. Interestingly, extended X-ray absorption fine structure (EXAFS) spectroscopy and X-ray photoelectron spectroscopy (XPS) studies suggested that the majority of the Ag atoms are located on the surface of the resulting clusters and Pd atoms are in the core region. The catalytic activity for 3-hexyne-1-ol hydrogenation was investigated and the AgPd@$SiO_2$ catalysts showed superior selectivity for the selective hydrogenation to 3-hexene-1-ol.

## Introduction

Design and fabrication of ligand-free nanomaterials is a special area of interest in catalysis because that enables one to avoid subsequent activation processes. Generally, bottom-up and top-down approaches have been reported for the synthesis of nanoparticles.[1] In the bottom-up approach, nanostructures are synthesized by assembling atoms and molecules. The chemical reduction method is the most common and simple bottom-up approach for the synthesis of nanostructures that involves the reduction of metal salts using various reducing agents in the presence of molecular or polymer capping agents. The presence of a capping agent blocks the active sites on the metal surface which affects the activity and selectivity of catalysts.[2] Although it is possible to remove the capping agents through an activation process, this often leads to sintering and the subsequent deactivation of the catalyst.[3] On the other hand, in top-down approaches nanostructures are fabricated by slicing or breaking apart a bulk material. Micro-patterning, pyrolysis, thermal decomposition, and milling are commonly used techniques for the top-down fabrication of metal nanostructures.[4] Nanostructures synthesized *via* top-down approaches possess a definite advantage over chemically synthesized nanoparticles *via* bottom-up strategies as they have clean surfaces which is essential for catalysis. Despite this attractive feature, several challenges such as the complexity of the synthetic procedure, the poorer ability to control size and shape of nanomaterials, and the use of sophisticated techniques limit the application of top-down approaches in nanoparticle synthesis.[5]

Thermal decomposition is most convenient and easiest top-down approach for nanoparticle synthesis.[6,7] Wang *et al.* demonstrated a simple method for the synthesis of monodispersed spherical colloids from the low melting metals such as Pb, In, Sn, Cd, and Bi.[8] By taking advantage of the thermal decomposition of Bi metal, nanoparticles with diameters in the range of 100–600 nm are synthesized by emulsifying molten drops of Bi in boiling di(ethylene glycol) followed by quenching with cold ethanol. Jung *et al.* demonstrated that Ag nanoparticles with an average size of 6.2 ± 1.2 nm can be synthesized using Ag metal as a precursor in a ceramic heater by an evaporation–condensation process.[9] Others have shown that the surface of Ag nanoparticles are easily oxidized to $AgO_x$ during annealing in air.[10,11] However, $AgO_x$ is thermodynamically unstable and dissociates into Ag and $O_2$ above ~300 °C. Previously our group synthesized Ag clusters with an average size of 2.3 ± 0.4 nm by the thermal decomposition of silica-encapsulated Ag nanotriangles in air.[12]

There has been significant interest in the synthesis of Ag nanostructures because they can serve as a sacrificial template

[a] 110 Science Place, Department of Chemistry, University of Saskatchewan, S7N 5C9, Canada. E-mail: robert.scott@usask.ca
[b] Department of Chemistry, Mississippi State University, 39762-9573, USA

† Electronic supplementary information (ESI) available: UV-vis spectra of Ag nanotriangles, BET surface area of Ag@$SiO_2$ calcined at 650 °C, TEM image of Pd@$SiO_2$, and XPS survey scan. See DOI: 10.1039/d0cy01675f

Published on 29 October 2020. Downloaded by University of New England on 11/9/2020 7:05:56 PM.

for the synthesis of various bimetallic nanostructures *via* galvanic replacement. The driving force for galvanic reactions is the redox potential difference between two metal atoms, *i.e.* the metal with lower redox potential is typically replaced by another metal atom. For example, Ag ($E^{\circ}_{1/2}$ $Ag^{+}$, Ag = 0.79 V) can be oxidized with metal salts of Au ($E^{\circ}_{1/2}$ $Au^{3+}$, Au = 1.49 V), Pt ($E^{\circ}_{1/2}$ $Pt^{2+}$, Pt = 1.18 V) and Pd ($E^{\circ}_{1/2}$ $Pd^{2+}$, Pd 0.95 V).[13] A number of groups have synthesized AgPd, AgAu and AgPt bimetallic catalysts *via* galvanic reactions using Ag as a sacrificial template.[14–20] This method enables the synthesis of a broad range of hollow and porous nanostructures from Ag templates with different morphologies that includes nanoboxes, nanoprisms, and nanocages.[20–23] Many studies show that dispersion of Pd atoms on a second metal promotes the selectivity of hydrogenation reaction.[24–27] Tedsree *et al.* synthesized a series of core–shell M@Pd catalysts (M = Ag, Au, Rh, Pt and Ru) and observed that Ag nanoparticles coated with a thin layer of Pd atoms are the most effective catalysts for $H_2$ production from formic acid decomposition.[28] The improvement in catalytic activity that was seen in Ag@Pd catalysts is due to the electronic modification of the Pd shell by the Ag core. AgPd bimetallic catalysts were found to be more active for the 4-nitrophenol reduction reaction than their monometallic systems.[29] Pei *et al.* observed a significant improvement in selectivity for acetylene hydrogenation by alloying Pd with Ag.[30] Interestingly, Ag alloy Pd-single atom catalysts showed higher activity and selectivity towards ethylene than the monometallic $Pd/SiO_2$ and $Ag/SiO_2$ catalysts. Previously our group reported the synthesis of Ag–Pd core–shell catalysts by galvanic replacement of polyvinylpyrrolidone-stabilized Ag nanoparticles with $K_2PdCl_4$.[31] While atom-precise Ag clusters can be made using thiolate stabilizers, activating such clusters for catalysis without sintering is very challenging.[3,32] Top-down strategies that create highly disperse Ag clusters without ligands on their surfaces which can then be used as templates for the formation of bimetallic nanoparticles are needed.

Herein we report a procedure to synthesize AgPd bimetallic catalysts from $Ag@SiO_2$ catalysts that are created by the thermal decomposition of larger Ag nanomaterials inside silica shells. The reduction of Pd(II) salts was monitored through using *in situ* Pd $L_3$-edge XANES using a liquid cell. XPS and EXAFS analysis provided clear evidence for the formation of bimetallic clusters. Low first shell coordination numbers of Ag in the EXAFS analysis suggested that Ag atoms are predominantly located on the surface of a Pd core. The catalytic activity for 3-hexyne-1-ol hydrogenation was investigated and the bimetallic $AgPd@SiO_2$ catalysts showed a superior selectivity to 3-hexene-1-ol compared to the monometallic counterparts.

# Experimental

## Materials

Silver nitrate ($AgNO_3$, ≥99%, Sigma-Aldrich), 16-mercatptohexadecanoic acid (MHA, 95%, Sigma-Aldrich), trisodium citrate (96%, EMD), potassium tetrachloropalladate(II) ($K_2PdCl_4$, 98%, Aldrich), 11-mercaptoundecanoic acid (MUA, 95%, Sigma-Aldrich), sodium borohydride ($NaBH_4$, 98%, Alfa Aesar), acetone ($C_3H_6O$, 99.5%, Fischer Scientific), *o*-phosphoric acid ($H_3PO_4$, 85%, Fischer Scientific), methylene chloride ($CH_2Cl_2$, 99.5%, Fischer Scientific), tetraethylorthosilicate (TEOS, 98%, Aldrich), hydrogen peroxide ($H_2O_2$, 30%, Fischer Scientific), poly(*N*-vinylpyrrolidone (PVP, 40 000 g $mol^{-1}$, Alfa Aesar), and dimethylamine (DMA, 40%, Sigma-Aldrich) were used as received. Ammonia (30%), tetrahydrofuran (THF, high purity) and ethanol (100%) were purchased from EMD, Fisher Scientific and Commercial Alcohols, respectively.

## Synthesis of Ag encapsulated with silica

The procedure for the synthesis of silica encapsulated Ag nanotriangles has been documented previously.[33,34] Briefly, $AgNO_3$ (500 μL, 50 mM), trisodium citrate (5 ml, 75 mM), PVP (1 mL, 17.5 mM), and $H_2O_2$ (30%, 600 μL) were added to 248 mL of deionized water. Then, $NaBH_4$ was added to the solution and the solution was stirred until it turned from yellow to blue. After this, the Ag nanotriangles were collected by centrifugation at 8500 rpm for 2.0 h. The Ag nanotriangles were then redispersed in 100 mL of deionized water, followed by the addition of ethanolic MHA (1.5 mL, 5.0 mM). After stirring for 10 min, MHA-functionalized Ag triangles were collected by centrifugation (8500 rpm, 2.0 h). The Ag nanotriangles were then dispersed into an ethanolic TEOS solution (20 mL, 16 mM) and stirred for 2 min. To this solution, aqueous DMA (2 mL, 20% w/v) was added, and the resulting solution was stirred at 200 rpm for 12 h. The final material was removed from the solution by centrifugation and washed several times with water and ethanol. The resulting materials were dried in an oven at 100 °C followed by calcination in a Lindberg/Blue M tube furnace at 650 °C in air for 15 min with a ramping rate of 10 °C $min^{-1}$. For brevity, the resulting Ag nanotriangles encapsulated with silica and calcined at 650 °C are designated as $Ag@SiO_2$. The metal loading was found to be 2.0% by AAS analysis.

## Synthesis of $AgPd@SiO_2$ bimetallic catalysts by galvanic exchange with Pd precursor

20 mg of $Ag@SiO_2$ ([Ag] = $4.0 \times 10^{-3}$ mmol) was dispersed in water followed by the addition of $K_2PdCl_4$ (200 μl, 0.020 M). The solution was stirred for 1 h. The resulting black coloured material was collected by centrifugation and washed with deionized water. The AgPd bimetallic catalyst ($AgPd@SiO_2$) was dried in an oven at 100 °C.

## Synthesis of $Pd@SiO_2$ catalyst

$Pd@SiO_2$ catalysts were made using the following procedure.[35] $K_2PdCl_4$ (20 mg, 0.06 mmol) was dissolved in $H_2O$ (2 mL). To this clear brown solution, acetone (10 mL) was added, which changed the solution color to a clear orange. Next, $H_3PO_4$ (250 μL) was added, followed by MUA (7

 This journal is © The Royal Society of Chemistry 2020

Published on 29 October 2020. Downloaded by University of New England on 11/9/2020 7:05:56 PM.

mg, 0.03 mmol). The solution was stirred for 5 min, then cooled in an ice bath. After cooling, a solution of $NaBH_4$ (23.2 mg, 0.613 mmol) in $H_2O$ (1 mL) was added, and the solution immediately became black. After stirring for an additional 5 min, the ice bath was removed, and the solution was stirred at room temperature for 5 min. The acetone was removed by vacuum at room temperature and the solid black product was collected by centrifugation. The solid was washed with methylene chloride and water and left to dry at room temperature. The resulting $Pd_m(MUA)_n$ clusters (10 mg) were dissolved in a minimal amount of tetrahydrofuran, then diluted with ethanol (10 mL). This $Pd_m(MUA)_n$ solution (0.25 mL) was added to a stirred solution of ethanol (10 mL) and TEOS (10 μL, 0.04 mmol). The solution was stirred for 1 min, then $NH_4OH$ (1 mL) was added. The final solution was stirred for 12 h. The dark brown product was collected by centrifugation, then washed with $H_2O$ and ethanol. The product was left to dry at room temperature. The dried $Pd_m(MUA)_n$@$SiO_2$ particles were calcined in air at 350 °C for 3 h. The catalyst was reduced by calcination at 250 °C under 5% $H_2$ in $N_2$ for 1 h to give Pd@$SiO_2$.

### Characterization

Samples were analyzed by a Hitachi HT7700 TEM operating at 100 kV. All samples were dispersed in ethanol and drop-casted on a Cu grid coated with carbon film. ImageJ software was used to measure the size of 100 particles for particle size distribution histograms.[36] The Brunauer–Emmett–Teller (BET) surface area and pore size distribution of the Ag@$SiO_2$ catalysts were performed on an ASAP 2010 Micrometrics instrument. Prior to the analysis, the catalyst was degassed under vacuum at 200 ± 2 °C and nitrogen adsorption analysis was conducted at −196 °C. Metal loading was analyzed by a Varian Spectra AA 55 atomic absorption spectroscope. UV-vis spectra of Ag nanotriangles were recorded on a Varian Cary 50 Bio UV-vis spectrometer. Pd $L_3$ edge spectra were collected at the soft X-ray micro characterization beamline (SXRMB) at the Canadian Light Source. For *in situ* measurements, the Pd precursor (1.0 mL, 0.020 M) aqueous solution was sealed in a liquid cell (SPEX CertiPrep Disposable XRF X-Cell sample cups) and was covered with an Ultralene® thin film. The liquid cell was placed inside an aluminum chamber. A magnetic stirrer was used for stirring and all the measurements were carried out under He atmosphere. Extended X-ray absorption spectra fine structure (EXAFS) spectroscopic analysis was performed on the HXMA beamline 061D-1 (energy range 5–30 keV, resolution $1 \times 10^{-4}$ $\Delta E/E$) at the Canadian Light Source. All data was collected in fluorescence mode using a 32-element detector. The energy for the Ag K edge (25 514 eV) and Pd K edge (24 350 eV) was selected by using a Si monochromator. All samples were mixed with boron nitride and then pressed into pellets before analysis. Higher harmonics were removed by detuning the double crystal monochromator. Data analysis and EXAFS fitting were carried out using the Demeter software package.[37] To fit the Ag and Pd data, an amplitude reduction factor was obtained from fitting of the corresponding metal foils. The amplitude reduction factor for both Pd and Ag were found to be 0.81. The coordination number of samples was determined by keeping this amplitude reduction factor fixed. All XPS measurements were collected using a Kratos (Manchester, UK) system equipped with a 500 mm Rowland circle monochromated Al $K_\alpha$ (1486.6 eV) source and combined hemispherical analyzer (HSA) and spherical mirror analyzer (SMA). The largest spot size (hybrid slot setting) was used to collect the data, which is approximately a beam size of 300 × 700 microns. All survey scan spectra were collected in the 0–1200 binding energy range in 1 eV steps with a pass energy of 160 eV. High-resolution scans of multiple regions were conducted using 0.1 eV steps with a pass energy of 20 eV. An accelerating voltage of 15 keV and an emission current of 15 mA was used for the analysis. The operating vacuum pressure was less than $1 \times 10^{-8}$ Torr. The spectra were referenced to a standard C 1s binding energy of 284.4 eV. All spectra were fitted using Casa XPS software.[38] $^1$H nuclear magnetic resonance (NMR) were recorded with a Bruker 500 MHz Avance spectrometer, with $CDCl_3$ as the solvent. The FTIR spectra was performed with a Bruker TENSOR 27 equipped with an attenuated total reflection (ATR) sampler.

### Catalytic measurements for 3 hexyne-1-ol hydrogenation

Hydrogenation reactions were carried out in a 50 mL round-bottom flask under $H_2$ atmosphere. 20 mg of the catalyst was dispersed in 5.0 mL of a water/ethanol (4 : 1) mixture, and 100 μL of 3-hexyne-1-ol was added to start the reaction. The reaction mixture was stirred at room temperature for 3 h. Prior to the $^1$H NMR analysis, the products were extracted from the reaction solution with 2 mL aliquots of $CDCl_3$. For the recyclability test, catalysts were recovered from the reaction mixture by centrifugation, washed with acetone and dried at 50 °C.

## Results and discussion

The UV-vis absorption spectra of the Ag nanotriangles (Fig. S1†) shows three peaks, at 334 nm, 430 nm, and an intense peak centred at 538 nm that could be assigned to out-plane quadrupole resonances, in-plane quadrupole, and in-plane dipole resonance of the Ag nanotriangles, respectively.[39] Fig. 1a shows a TEM image of the Ag nanotriangles, note that the nanotriangles are randomly oriented and thus some appear to be non-triangular in shape, particularly as their width is quite small. The TEM image of as-synthesized Ag@$SiO_2$ (Fig. 1b) indicates that Ag nanotriangles are encapsulated in a silica shell. The average Ag nanotriangle size is 19 ± 4 nm and the silica shell thickness is 80 ± 10 nm. Others have shown that the concentration of the TEOS precursor has a significant role in controlling the thickness of the silica shell.[40,41] After calcination at 650 °C, the Ag nanotriangles are fragmented into small particles, as shown in Fig. 1c. The average Ag particle size in the resulting

Published on 29 October 2020. Downloaded by University of New England on 11/9/2020 7:05:56 PM.

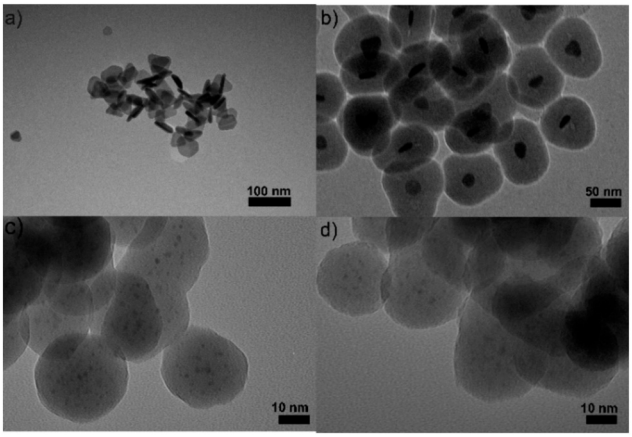


**Fig. 1** TEM images of a) as-synthesized Ag NPs, b) as-synthesized Ag@$SiO_2$, c) Ag@$SiO_2$ calcined at 650 °C, and d) Ag–Pd@$SiO_2$ sample after galvanic exchange.

materials is 2.5 ± 0.5 nm. These results agree with previous work that investigated the thermal degradation of silica encapsulated Ag nanotriangles by *ex situ* TEM and EXAFS analysis.[12] It was proposed that atoms at the tips of the Ag nanotriangles are easily oxidized to $AgO_x$ during annealing in air. However, $AgO_x$ is thermodynamically unstable. At higher temperatures (above ~300 °C) it dissociates back into Ag and $O_2$.[11] Previous results suggested that the oxygen atmosphere has a crucial role in the fragmentation process, as no such dispersion of Ag was seen in inert atmospheres.

The porous nature of the Ag@$SiO_2$ materials was evaluated by a nitrogen adsorption/desorption isotherm, which is shown in Fig. S2.† The BET surface area of the Ag@$SiO_2$ materials was found to be 97 $m^2$ $g^{-1}$ and the BJH desorption average pore width was 24.5 nm. The thermal treatment at 650 °C leads to the removal of protecting ligands and solvent, which leads to disordered mesoporosity; similar results have been seen by other groups.[42–44] The final porosity of the materials should allow the accessibility of Pd precursor to the silver atoms for the galvanic replacement reaction. Previously we have shown that the thermal treatment of silica encapsulated $Au_{25}(MUA)_{18}$ clusters at 250 °C for 3 h leads to the removal of thiol ligands and results in an increase of surface area from 24 $m^2$ $g^{-1}$ to 70 $m^2$ $g^{-1}$.[45] To verify the removal of thiol ligands during the thermal treatment, FTIR spectra (Fig. S3†) were collected. As-synthesized Ag@$SiO_2$ and Pd@$SiO_2$ materials show $CH_2$ symmetric and $CH_2$ asymmetric stretch modes around 2855 and 2940 $cm^{-1}$.[46,47] A small peak was observed at 2555 $cm^{-1}$ which is a characteristic feature of S–H stretching. In addition, the FTIR spectrum shows features around 1683 $cm^{-1}$, which are related to the carbonyl group of the carboxylic acid. The characteristic features associated with the thiol ligands were not observed in the calcined samples, which indicates the removal of ligands from the catalysts.

The AgPd@silica catalysts were synthesized by redispersing the calcined Ag@$SiO_2$ sample and by galvanically exchanging the core Ag using excess Pd(II). After the addition of $K_2PdCl_4$, the colour of the material turned from yellow to black which is consistent with the reduction of the Pd salt. The complete replacement reaction of Ag with Pd precursor can be described as $2Ag + Pd^{2+} \rightarrow Pd + 2Ag^{+}$. A TEM image of the resulting AgPd@$SiO_2$ sample is shown in Fig. 1d. The average particle size was measured to be 2.6 ± 1.3 nm. The final metal composition of Ag–Pd@silica samples was examined by AAS analysis which indicates the sample has 1.0% Pd and 0.1% Ag content. To compare the catalytic activity, Pd@$SiO_2$ materials were also made directly with a similar 1.0% metal loading which was confirmed by AAS analysis. The average particle size of Pd@$SiO_2$ catalysts was measured to be 2.2 ± 0.8 nm (Fig. S4†).

XPS measurements were performed to probe the composition and chemical state of Ag and Pd in the silica matrix. Fig. 2a shows the XPS spectrum of the Ag@$SiO_2$ starting material. The Ag $3d_{5/2}$ and Ag $3d_{3/2}$ peaks were seen at 368.3 eV and 374.3 eV. These values are in good agreement with reported values for metallic Ag.[48] Thus Ag clusters remain in the zerovalent state after calcination and the presence of oxidized Ag can be ruled out. The atom percentage of Ag as determined by XPS was reduced from 0.5% to 0.1% (Fig. S5 and Table S1†) after the galvanic exchange with Pd. Fig. 2b and c show the XPS spectrum of the final Ag–Pd@$SiO_2$ materials. The Ag $3d_{5/2}$ and Ag $3d_{3/2}$ peaks appear at 367.8 eV and 373.8 eV, respectively.[48] The Pd 3d XPS spectrum consists of Pd $3d_{5/2}$ and Pd $3d_{3/2}$ peaks at 334.5 eV and 339.6 eV corresponding to the binding energy of metallic Pd.[49] The signal-to-noise for the Pd XPS is much poorer (despite the presence of significantly more Pd than Ag seen in AAS results), possibly due to a negligible amount of Pd on the surface of the particles.[50] The XPS results show evidence for the complete reduction of $Pd^{2+}$ to zerovalent Pd oxidation state. The Ag 3d spectra are red-shifted by 0.5 eV in comparison to that of pure Ag@$SiO_2$ catalysts, while the Pd 3d peaks also show a redshift by 0.5 eV which may be due to electronic AgPd interactions in the bimetallic clusters.[51–53] As Pd is more electronegative than Ag, charge transfer would be expected from Ag to Pd.[54] As a result, Pd would be expected to shift to lower binding energy and Ag to higher binding energy. The negative shift of both Pd and Ag has previously been observed in the AgPd alloy system and was explained by Abrikosov *et al.* in terms of an inter-atomic charge redistribution due to valence electron distribution.[55]

XANES spectroscopy can be used for monitoring changes in the oxidation state of materials, whereas the EXAFS technique provides information about the local structure around the absorbing atom. In the XANES region, the white line intensity of the Pd $L_3$ edge spectra is directly related to the number of vacancies in the Pd 4d-band.[56] The Pd $L_3$ edge represents the $2p_{3/2}$ to 4d allowed transition which is sensitive to the oxidation state and vacancy change of the valance d band. The adsorption edge energy also typically increases as the oxidation state of the metal increases. A change in white line intensity, along with a slight edge energy shift reflects a change in the oxidation state of the Pd. The

 This journal is © The Royal Society of Chemistry 2020

Published on 29 October 2020. Downloaded by University of New England on 11/9/2020 7:05:56 PM.

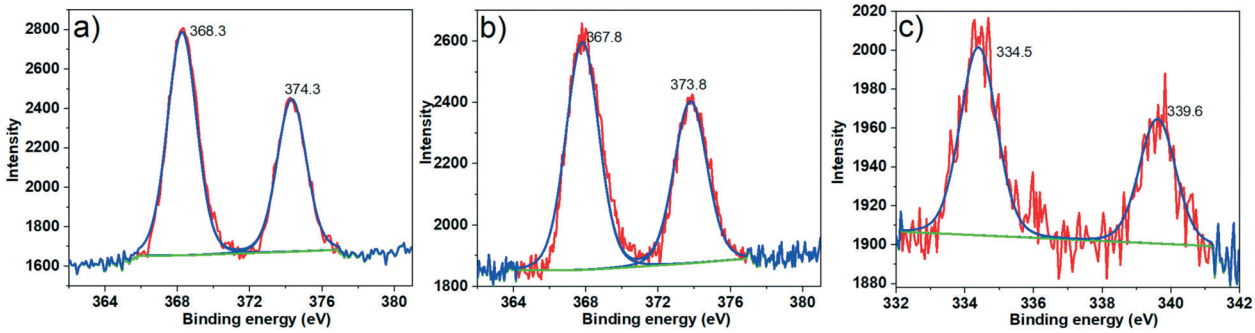


Fig. 2 a) Ag 3d XPS spectra of Ag@$SiO_2$, b) Ag 3d XPS spectra of AgPd@$SiO_2$ and c) Pd 3d XPS spectra of AgPd@$SiO_2$.

galvanic reaction between $K_2PdCl_4$ and Ag clusters (Ag@$SiO_2$) was monitored by *in situ* XANES spectra at the Pd $L_3$ edge using a liquid cell set up for *in situ* XAS studies developed at the SXRMB beamline at the Canadian Light Source.[57] The *in situ* XAS spectra of the Pd salt solution before and after the addition of Ag@$SiO_2$ is shown in Fig. 3. A prominent white line was observed for the $K_2PdCl_4$ solution which is an indication of the presence of Pd(II). After the addition of Ag@$SiO_2$, the white line intensity at the Pd $L_3$-edge spectra decreased significantly, which is an indication of the reduction of Pd(II) to Pd(0). The final XANES spectrum closely resembles a Pd foil spectrum, thus suggesting that Pd is being fully reduced to the zerovalent state. This provides direct evidence for the galvanic reaction of $K_2PdCl_4$ with zerovalent Ag clusters.

EXAFS analysis at both the Pd and Ag K edges was carried out in fluorescence mode on the hard X-ray microanalysis (HXMA) beamline at CLS. Fig. 4 shows the Ag and Pd K edge EXAFS data in *k*-space for the AgPd@$SiO_2$ sample. The amplitude decreases for the Ag–Pd@$SiO_2$ sample as compared to bulk Ag and Pd foil, respectively, suggesting that small clusters were formed that have a large fraction of atoms on the surface. The periodicity of the EXAFS oscillation pattern for AgPd@$SiO_2$ at both the Ag and Pd K edge was observed to be slightly different than the respective foils which indicates the presence of bimetallic clusters. A face-centered cubic alloy model was used to fit Ag and Pd K edge data, and the fitting results at the *k*- and *R*-space are shown in Fig. 5. Since Pd and Ag have similar atomic numbers, their backscattering and phase effects on the photoelectron wave is nearly identical, and thus it is very difficult to distinguish between these species around the central atom. Since the scattering of Ag–Ag and Ag–Pd are similar, general coordination numbers $N_{Pd-M}$ and $N_{Ag-M}$ were fit (whereas M is Ag or Pd). Black and red lines represent the experimental data and simulated EXAFS fit respectively. The EXAFS fit parameters that were obtained from 1st shell modelling are shown in Table 1. The modeled Ag–Ag distance of 2.83(1) Å is slightly shorter than the typical Ag–M distance in Ag foil (2.88 Å). Similarly, the Pd–M first shell distance of 2.799(9) Å is longer than typically seen for Pd foil ($R$ = 2.75 Å). These dissimilarities in interatomic distances are strong indicators of the presence of heteroatomic bonding in Ag–Pd catalysts.[58–60]

The average coordination number for the Ag–M and Pd–M shell was found to be 3.3(1) and 8.7(9) respectively. The low coordination number of Ag–M shell suggests that the majority of the Ag atoms are present on the Pd surface.[61,62] The CN of 3.3(1) for Ag–M contribution is likely due to the presence of Ag atoms on the edges or corners of the clusters. The presence of Ag atoms on the surface and Pd atoms in the core is also consistent with XPS analyses. By combining EXAFS, XPS and AAS results, it seems that the majority of the

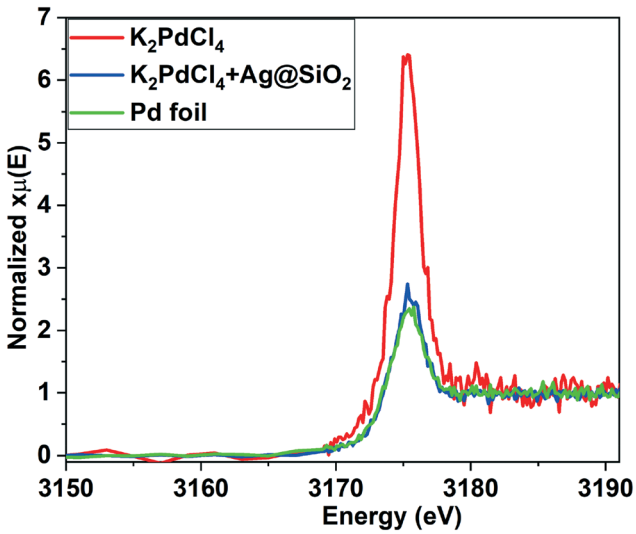


Fig. 3 *In situ* Pd $L_3$-edge XANES spectra of $K_2PdCl_4$ before and after the addition of Ag@silica.

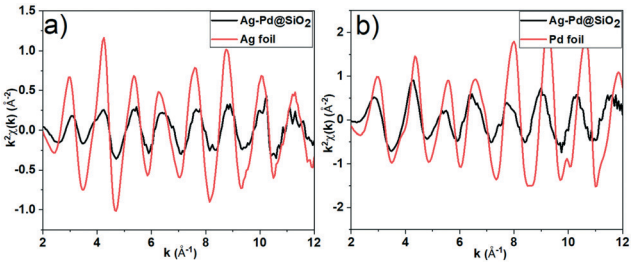


Fig. 4 EXAFS data in *k* space AgPd@$SiO_2$ samples at a) the Ag K edge, and b) the Pd K edge.

Published on 29 October 2020. Downloaded by University of New England on 11/9/2020 7:05:56 PM.

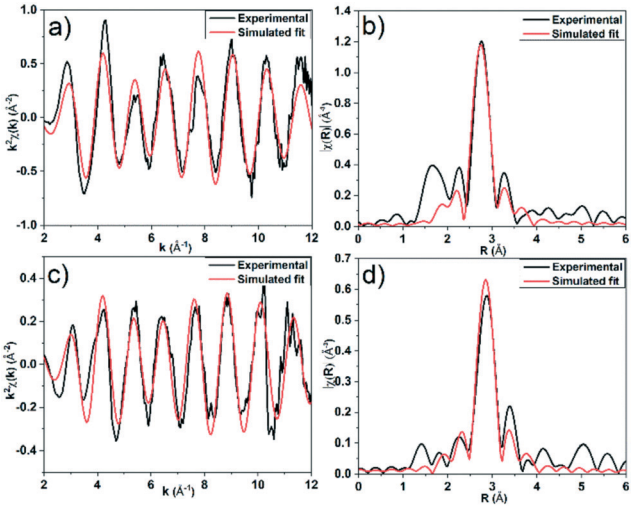


**Fig. 5** EXAFS fitting data of AgPd@$SiO_2$; a) Pd K edge in *k*-space, b) Pd K edge in *R*-space, c) Ag K edge in *k* space, and d) Ag K edge in *R* space.

**Table 1** EXAFS fitting parameters of AgPd@$SiO_2$ catalyst

| | Type | CN | *R*/Å | $\sigma^2$/Å$^2$ | $E_o$ shift (eV) |
|---|---|---|---|---|---|
| Pd | Pd–M | 8.7(9) | 2.799(9) | 0.009(1) | −2.2(8) |
| Ag | Ag–M | 3.3(1) | 2.83(1) | 0.006(1) | −0.6(9) |

Ag atoms are located on the surface of the bimetallic clusters, while Pd atoms are predominantly in the core region.

Pd catalysts are widely used for hydrogenation reactions, but when used for substrates such as 3-hexyn-1-ol typically show poor selectivity to alkenes due to over-hydrogenation.[63] Active site isolation by addition of other metals is an efficient way to improve the selectivity to 3-hexen-1-ol.[31] To analyze the catalytic activity and selectivity of the catalysts, the hydrogenation reaction of 3-hexyn-1-ol was evaluated over Ag@$SiO_2$, Pd@$SiO_2$, and Ag–Pd@$SiO_2$ catalysts, and results are shown in Table 2. No catalytic activity was observed using Ag@$SiO_2$. The activity was slightly higher in the case of the pure Pd@$SiO_2$ as compared to AgPd@$SiO_2$. However, the monometallic Pd@$SiO_2$ catalyst also promoted the over-hydrogenation and gave the undesired hexanol product. This result is consistent with the work of others that has shown that Pd catalysts are poorly selective for alkyne hydrogenations.[24,30,64–66] Interestingly, after the addition of Pd to Ag@$SiO_2$, the catalyst became active for the hydrogenation reaction. A significant selectivity difference was observed for Pd@$SiO_2$ and AgPd@$SiO_2$ catalysts for the hydrogenation reaction. To analyze the selectivity of the catalyst over time, the time dependent hydrogenation reaction of 3-hexyn-1-ol was evaluated for the AgPd@$SiO_2$ catalyst, and results are shown in Fig. S6.† The selectivity for the 3-hexen-1-ol was found to be maintained for the AgPd@$SiO_2$ catalysts over time. The promotional effect that was observed in AgPd catalysts is due to the synergetic effect of bimetallic AgPd nanoparticles for selective hydrogenations,

**Table 2** The catalytic activity for 3-hexyne-1-ol hydrogenation reaction

| Catalysts | Ag : Pd ratio[a] | Conversion % | Selectivity % | |
|---|---|---|---|---|
| | | | 3-Hexen-1-ol | Hexan-1-ol |
| Ag@$SiO_2$ | 2.0 : 0.0 | 0.0 | — | — |
| Ag–Pd@$SiO_2$ | 0.1 : 1.0 | 43.0 | 90.7 | 9.3 |
| Pd@$SiO_2$ | 0.0 : 1.0 | 47.6 | 67.6 | 32.4 |

[a] Ag : Pd ratio from AAS analysis. The 3-hexyne-1-ol hydrogenation reaction (100 μL) was performed at room temperature for 3 h using 20 mg of the catalyst with 1.0% wt Pd loading.

as the presence of Ag atoms suppresses the full hydrogenation product and increases selectivity to 3-hexen-1-ol.[67] Mei *et al.* investigated the role of Ag on the Pd surface in selective hydrogenation of acetylene–ethylene mixtures over Pd and bimetallic PdAg alloy as model catalysts.[68] They found that the presence of Ag on the Pd surface weakens the binding strengths of all surface intermediates and therefore increases their rates of desorption as well as their rates of hydrogenation. Ag enhanced the desorption of ethylene and hydrogen from the catalyst surface and suppressed further hydrogenation. Mitsudome *et al.* reported that modification of Pd nanoparticles with Ag suppresses the over-hydrogenation of alkynes to alkanes.[69] They found that Ag–Pd core–shell structures are active for the semi-hydrogenation of 1-octyne under 1 bar $H_2$ at room temperature resulting in selectivity towards the alkene of 99%. The Pd core act as an $H_2$ source and the Ag shell served as the surface for the semi-hydrogenation of the alkyne resulting in a reduction of the intrinsically low alkene-selectivity of Pd by inhibiting the contact between Pd and the alkenes. Previously we investigated the selective hydrogenation of 3-hexyne-1-ol over AgPd catalysts synthesized *via* galvanic exchange reaction of Ag nanoparticle seeds (3 nm) with $K_2PdCl_4$.[31] The catalytic activity and selectivity of catalysts with different Ag : Pd ratio was investigated and the catalysts with Ag : Pd ratios of 2 : 1 were found to be the most active catalysts, with high selectivity to *cis*-3-hexen-1-ol. The activity of the AgPd@$SiO_2$ catalyst was maintained for four consecutive cycles (Table S2†), which indicates that the silica shell helps promote the recyclability of the catalyst. This result is in good agreement with our previous recyclability studies using silica-encapsulated $Au_{25}(MUA)_{18}$ clusters for styrene epoxidation reactions.[45]

## Conclusions

AgPd bimetallic catalysts were prepared *via* a top-down approach from Ag cluster dispersions broken down from larger Ag nanoparticles, followed by galvanic replacement of Ag with Pd. *In situ* XANES spectroscopy showed that all Pd was reduced during the galvanic replacement of $K_2PdCl_4$ with the Ag clusters. EXAFS spectroscopy and XPS studies suggested that the majority of the Ag atoms are located on the surface of the resulting bimetallic clusters and Pd atoms are in the core

 This journal is © The Royal Society of Chemistry 2020

Published on 29 October 2020. Downloaded by University of New England on 11/9/2020 7:05:56 PM.

region. The catalytic activity for the 3-hexyn-1-ol hydrogenation reaction was investigated. AgPd catalysts derived from Ag@$SiO_2$ showed better selectivity to 3-hexen-1-ol than their monometallic counterparts, which indicates the electronic interactions of Pd with Ag atoms suppresses the over-hydrogenation of 3-hexyn-1-ol. The resulting catalysts could be easily recycled with similar selectivity over multiple cycles.

## Conflicts of interest

There are no conflicts to declare.

## Acknowledgements

We would like to acknowledge the National Sciences and Engineering Research Council of Canada (NSERC) for financial support. We thank Ning Chen and Yongfeng Hu at the Canadian Light Source (CLS) for assistance with XAS measurements. We also thank Dr. Pia Wennek for assistance with FTIR measurements. EXAFS and *in situ* XANES experiments described in this paper were performed at the Canadian Light Source, which is supported by the Natural Sciences and Engineering Research Council of Canada, the National Research Council Canada, the Canadian Institutes of Health Research, the Province of Saskatchewan, Western Economic Diversification Canada, and the University of Saskatchewan.

## Notes and references

1 P. Iqbal, J. A. Preece and P. M. Mendes, *Supramol. Chem.*, 2012, **6**, 1–12.
2 X. Nie, H. Qian, Q. Ge, H. Xu and R. Jin, *ACS Nano*, 2012, **6**, 6014–6022.
3 V. Sudheeshkumar, K. O. Sulaiman and R. W. J. Scott, *Nanoscale Adv.*, 2020, **2**, 55–69.
4 V. Pareek, A. Bhargava, R. Gupta, N. Jain and J. Panwar, *Nanoscale Adv.*, 2017, **9**, 527–544.
5 M. Pelton, J. Aizpurua and G. Bryant, *Laser Photonics Rev.*, 2008, **2**, 136–159.
6 D. K. Lee and Y. S. Kang, *ACS Nano*, 2004, **26**, 252–256.
7 L. Gharibshahi, E. Saion, E. Gharibshahi, A. H. Shaari and K. A. Matori, *Materials*, 2017, **10**, 402.
8 Y. Wang and Y. Xia, *Nano Lett.*, 2004, **4**, 2047–2050.
9 J. H. Jung, H. Cheol Oh, H. Soo Noh, J. H. Ji and S. Soo Kim, *J. Aerosol Sci.*, 2006, **37**, 1662–1670.
10 Z. W. Lei, M. Liu, W. Ge, Z. P. Fu, K. Reinhardt, R. J. Knize and Y. Lu, *Appl. Phys. Lett.*, 2012, **101**, 083903.
11 K. Chatterjee, S. Banerjee and D. Chakravorty, *Phys. Rev. B*, 2002, **66**, 085421.
12 M. K. Gangishetty, R. W. J. Scott and T. L. Kelly, *Dalton Trans.*, 2016, **45**, 9827–9834.
13 D. R. Lide, *CRC Handbook of Chemistry and Physics*, CRC press, Boca Raton, FL, 2006.
14 W. Zhang, J. Yang and X. Lu, *ACS Nano*, 2012, **6**, 7397–7405.
15 B. G. Prevo, S. A. Esakoff, A. Mikhailovsky and J. A. Zasadzinski, *Small*, 2008, **4**, 1183–1195.
16 A. G. M. Silva, T. S. Rodrigues, V. G. Correia, T. V. Alves, R. S. Alves, R. A. Ando, F. R. Ornellas, J. Wang, L. H. Andrade and P. H. C. Camargo, *Angew. Chem., Int. Ed.*, 2016, **55**, 7111–7115.
17 T. S. Rodrigues, A. G. M. Silva, A. B. L. de Moura, I. G. Freitas and P. H. C. Camargo, *RSC Adv.*, 2016, **6**, 62286–62290.
18 A. G. M. da Silva, T. S. Rodrigues, S. J. Haigh and P. H. C. Camargo, *Chem. Commun.*, 2017, **53**, 7135–7148.
19 J. Chen, B. Wiley, J. McLellan, Y. Xiong, Z. Y. Li and Y. Xia, *Nano Lett.*, 2005, **5**, 2058–2062.
20 A. N. Chen, S. M. McClain, S. D. House, J. C. Yang and S. E. Skrabalak, *Chem. Mater.*, 2019, **31**, 1344–1351.
21 E. Sutter, K. Jungjohann, S. Bliznakov, A. Courty, E. Maisonhaute, S. Tenney and P. Sutter, *Nat. Commun.*, 2014, **5**, 4946.
22 M. Tsuji, T. Kidera, A. Yajima, M. Hamasaki, M. Hattori, T. Tsuji and H. Kawazumi, *CrystEngComm*, 2014, **16**, 2684–2691.
23 C. L. Lee, C. M. Tseng, R. B. Wu, C. C. Wu and S. C. Syu, *Electrochim. Acta*, 2009, **54**, 5544–5547.
24 M. R. Ball, K. R. Rivera-Dones, E. B. Gilcher, S. F. Ausman, C. W. Hullfish, E. A. Lebrón and J. A. Dumesic, *ACS Catal.*, 2020, **10**, 8567–8581.
25 H. Zea, K. Lester, A. K. Datye, E. Rightor, R. Gulotty, W. Waterman and M. Smith, *Appl. Catal., A*, 2005, **282**, 237–245.
26 Y. Zhang, W. Diao, C. T. Williams and J. R. Monnier, *Appl. Catal., A*, 2014, **469**, 419–426.
27 W. Huang, W. Pyrz, R. F. Lobo and J. G. Chen, *Appl. Catal., A*, 2007, **333**, 254–263.
28 K. Tedsree, T. Li, S. Jones, C. W. A. Chan, K. M. K. Yu, P. A. J. Bagot, E. A. Marquis, G. D. W. Smith and S. C. E. Tsang, *Nat. Nanotechnol.*, 2011, **6**, 302–307.
29 T. Zhang, L. Li, Z. Ye, Q. Yang, Y. Tian and X. Guo, *RSC Adv.*, 2018, **8**, 18252–18259.
30 G. X. Pei, X. Y. Liu, A. Wang, A. F. Lee, M. A. Isaacs, L. Li, X. Pan, X. Yang, X. Wang, Z. Tai, K. Wilson and T. Zhang, *ACS Catal.*, 2015, **5**, 3717–3725.
31 C. F. Calver, P. Dash and R. W. J. Scott, *ChemCatChem*, 2011, **3**, 695–697.
32 K. O. Sulaiman, V. Sudheeshkumar and R. W. J. Scott, *RSC Adv.*, 2019, **9**, 28019–28027.
33 M. K. Gangishetty, K. E. Lee, R. W. J. Scott and T. L. Kelly, *ACS Appl. Mater. Interfaces*, 2013, **5**, 11044–11051.
34 Q. Zhang, N. Li, J. Goebl, Z. Lu and Y. Yin, *J. Am. Chem. Soc.*, 2011, **133**, 18931–18939.
35 M. Cargnello, N. L. Wieder, P. Canton, T. Montini, G. Giambastiani, A. Benedetti, R. J. Gorte and P. Fornasiero, *Chem. Mater.*, 2011, **23**, 3961–3969.
36 C. A. Schneider, W. S. Rasband and K. W. Eliceiri, *Nat. Methods*, 2012, **9**, 671–675.
37 B. Ravel and M. Newville, *J. Synchrotron Radiat.*, 2005, **12**, 537–541.
38 J. Baltrusaitis, B. Mendoza-Sanchez, V. Fernandez, R. Veenstra, N. Dukstiene, A. Roberts and N. Fairley, *Appl. Surf. Sci.*, 2015, **326**, 151–161.

Published on 29 October 2020. Downloaded by University of New England on 11/9/2020 7:05:56 PM.

39 A. Amirjani, N. N. Koochak and D. F. Haghshenas, *Mater. Res. Express*, 2018, **6**, 036204.
40 D. Niu, Z. Ma, Y. Li and J. Shi, *J. Am. Chem. Soc.*, 2010, **132**, 15144–15147.
41 P. D. Nallathamby, J. Hopf, L. E. Irimata, T. L. McGinnity and R. K. Roeder, *J. Mater. Chem. B*, 2016, **4**, 5418–5428.
42 N. Zanganeh, V. K. Guda, H. Toghiani and J. M. Keith, *ACS Appl. Mater. Interfaces*, 2018, **10**, 4776–4785.
43 A. H. Habibi, R. E. Hayes and N. Semagina, *Catal. Sci. Technol.*, 2018, **8**, 798–805.
44 S. Kim, D. W. Lee, K. Y. Lee and E. A. Cho, *Catal. Lett.*, 2014, **144**, 905–911.
45 V. Sudheeshkumar, A. Shivhare and R. W. J. Scott, *Catal. Sci. Technol.*, 2017, **7**, 272–280.
46 S. Ristig, D. Kozlova, W. Meyer-Zaika and M. Epple, *J. Mater. Chem. B*, 2014, **2**, 7887–7895.
47 B. M. Amoli, S. Gumfekar, A. Hu, Y. N. Zhou and B. Zhao, *J. Mater. Chem.*, 2012, **22**, 20048–20056.
48 H. Zhang, G. Wang, D. Chen, X. Lv and J. Li, *Chem. Mater.*, 2008, **20**, 6543–6549.
49 P. Wu, Y. Huang, L. Kang, M. Wu and Y. Wang, *Sci. Rep.*, 2015, **5**, 14173–14173.
50 A. B. Vysakh, C. L. Babu and C. P. Vinod, *J. Phys. Chem. C*, 2015, **119**, 8138–8146.
51 D. A. Slanac, W. G. Hardin, K. P. Johnston and K. J. Stevenson, *J. Am. Chem. Soc.*, 2012, **134**, 9812–9819.
52 S. K. Sengar, B. R. Mehta and G. Gupta, *J. Appl. Phys.*, 2014, **115**, 124301.
53 N. G. Semaltianos, R. Chassagnon, V. Moutarlier, V. Blondeau-Patissier, M. Assoul and G. Monteil, *Nanotechnology*, 2017, **28**, 155703.
54 J. A. Alonso and L. A. Girifalco, *Phys. Rev. B: Condens. Matter Mater. Phys.*, 1979, **19**, 3889–3895.
55 I. A. Abrikosov, W. Olovsson and B. Johansson, *Phys. Rev. Lett.*, 2001, **87**, 176403.
56 T. K. Sham, *Phys. Rev. B: Condens. Matter Mater. Phys.*, 1985, **31**, 1888–1902.
57 Y. Yao, Y. Hu and R. W. J. Scott, *J. Phys. Chem. C*, 2014, **118**, 22317–22324.
58 M. Navlani-García, K. Mori, A. Nozaki, Y. Kuwahara and H. Yamashita, *Ind. Eng. Chem. Res.*, 2016, **55**, 7612–7620.
59 P. Verma, Y. Kuwahara, K. Mori and H. Yamashita, *J. Mater. Chem. A*, 2015, **3**, 18889–18897.
60 C. Hu, X. Mu, J. Fan, H. Ma, X. Zhao, G. Chen, Z. Zhou and N. Zheng, *ChemNanoMat*, 2016, **2**, 28–32.
61 C. H. Chen, L. S. Sarma, J. M. Chen, S. C. Shih, G. R. Wang, D. G. Liu, M. T. Tang, J. F. Lee and B. J. Hwang, *ACS Nano*, 2007, **1**, 114–125.
62 P. N. Duchesne and P. Zhang, *J. Phys. Chem. C*, 2014, **118**, 21714–21721.
63 H. Zhou, X. Yang, L. Li, X. Liu, Y. Huang, X. Pan, A. Wang, J. Li and T. Zhang, *ACS Catal.*, 2016, **6**, 1054–1061.
64 B. Coq and F. Figueras, *J. Mol. Catal. A: Chem.*, 2001, **173**, 117–134.
65 G. X. Pei, X. Y. Liu, A. Wang, L. Li, Y. Huang, T. Zhang, J. W. Lee, B. W. L. Jang and C. Y. Mou, *New J. Chem.*, 2014, **38**, 2043–2051.
66 Y. Cao, Z. Sui, Y. Zhu, X. Zhou and D. Chen, *ACS Catal.*, 2017, **7**, 7835–7846.
67 S. González, K. M. Neyman, S. Shaikhutdinov, H. J. Freund and F. Illas, *J. Phys. Chem. C*, 2007, **111**, 6852–6856.
68 D. Mei, M. Neurock and C. M. Smith, *J. Catal.*, 2009, **268**, 181–195.
69 T. Mitsudome, T. Urayama, K. Yamazaki, Y. Maehara, J. Yamasaki, K. Gohara, Z. Maeno, T. Mizugaki, K. Jitsukawa and K. Kaneda, *ACS Catal.*, 2016, **6**, 666–670.

 This journal is © The Royal Society of Chemistry 2020